

Radiative B Meson DecayYutaka Ushiroda
(for the Belle Collaboration)Department of Physics, Kyoto University,
Oiwake-cho Kitashirakawa Sakyo-ku, Kyoto, JAPAN**Abstract**

We have studied radiative B meson decays using data collected at the $\Upsilon(4S)$ resonance with the Belle detector at the KEKB e^+e^- storage ring. We measured the exclusive branching fractions to the $K^*(892)\gamma$ final states to be $\mathcal{B}(B^0 \rightarrow K^{*0}(892)\gamma) = (49.6 \pm 6.7 \pm 4.5) \times 10^{-6}$ and $\mathcal{B}(B^+ \rightarrow K^{*+}(892)\gamma) = (38.9 \pm 9.3 \pm 4.1) \times 10^{-6}$. The inclusive branching fraction is measured to be $\mathcal{B}(B \rightarrow X_s\gamma) = (3.39 \pm 0.53 \pm 0.42^{+0.51}_{-0.55}) \times 10^{-4}$. We searched for $B \rightarrow \rho\gamma$ decays and obtained an upper limit of $\mathcal{B}(B \rightarrow \rho\gamma)/\mathcal{B}(B \rightarrow K^*(892)\gamma) < 0.19$ (90% C.L.).

Contributed to the Proceedings of the 4th International Conference
on B Physics and CP Violation, 19-23 February 2001, Ise-Shima, Japan

1 Introduction

Radiative B meson decays are sensitive to non-Standard-Model contributions. A Standard Model (SM) branching fraction calculation for $B \rightarrow X_s\gamma$ that includes next-to-leading order QCD corrections has a precision of 10% [3]. Experimental measurements of the branching fraction are useful for identifying or limiting non-SM theories [4]. The $b \rightarrow d\gamma$ process may provide additional sensitivity to non-SM effects, a precise measurement of $|V_{td}/V_{ts}|$ and direct CP violation within the SM framework. The exclusive channel $B \rightarrow \rho\gamma$ can be distinguished from the $B \rightarrow K^*(892)\gamma$ signal utilizing good high momentum kaon identification devices.

We have analyzed a large data sample collected at the $\Upsilon(4S)$ resonance with the Belle detector [1] at the KEKB e^+e^- storage ring [2]. We used 6.1 million $B\bar{B}$ events for $B \rightarrow X_s\gamma$ analysis and 11 million for other analyses.

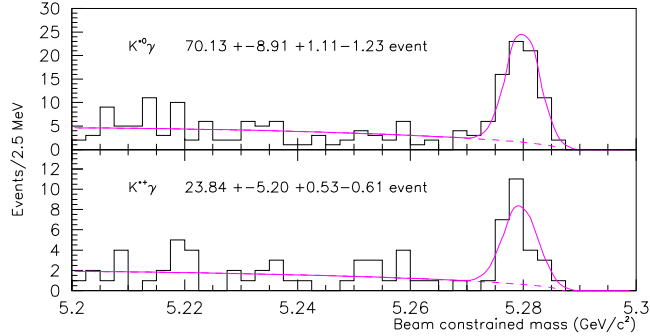


Figure 1: Beam constrained mass spectra for $B \rightarrow K^{*0}\gamma - K^{*0}\gamma$ (top) and $K^{*+}\gamma$ (bottom).

2 Analyses and Results

We have performed measurements of branching fractions for $B \rightarrow K^{*}(892)\gamma$, $B \rightarrow K_2^{*}(1430)\gamma$ and $B \rightarrow X_s\gamma$, and a search for $B \rightarrow \rho\gamma$. We also measured the partial rate asymmetry in $B \rightarrow K^{*}(892)\gamma$. We will give the results with descriptions for the essential part of analyses in the following subsections.

2.1 $B \rightarrow K^{*}(892)\gamma$

We did an exclusive reconstruction for $B \rightarrow K^{*}(892)\gamma$, where $K^{*}(892)$ is reconstructed from $K^{\pm}\pi^{\mp}$, $K_S^0\pi^0$, $K_S^0\pi^{\pm}$ and $K^{\pm}\pi^0$. A combined kaon-to-pion likelihood is constructed from the aerogel Čerenkov counters (ACC), the time-of-flight counter (TOF) and the dE/dx from the central drift chamber (CDC). A K/π separation cut is applied on the likelihood ratio. A $K\pi$ invariant mass window of $\pm 75 \text{ MeV}/c^2$ is taken around the nominal $K^{*}(892)$ mass. A likelihood ratio cut is applied in order to suppress the $q\bar{q}$ background, where the likelihood ratio is calculated from the B meson flight direction, the helicity angle of the $K^{*}(892)$ decay, and an event shape variable which we call *the Super Fox-Wolfram* (SFW). The SFW variable is a Fisher discriminant formed using Fox-Wolfram moments. The definition of SFW can be found in reference [5].

We extracted the signal yields by fitting the beam constrained mass (M_{bc}) distribution with an ARGUS function for the background and a Gaussian for the signal as shown in Figure 1. We determined the branching fractions to be

$$\mathcal{B}(B \rightarrow K^{*0}(892)\gamma) = (49.6 \pm 6.7 \pm 4.5) \times 10^{-6}$$

$$\mathcal{B}(B \rightarrow K^{*+}(892)\gamma) = (38.9 \pm 9.3 \pm 4.1) \times 10^{-6}.$$

We then checked the partial rate asymmetry,

$$A_{CP} = \frac{1}{1 - 2\eta} \cdot \frac{\mathcal{N}(\bar{K}^{*0}\gamma + K^{*-}\gamma) - \mathcal{N}(K^{*0}\gamma + K^{*+}\gamma)}{\mathcal{N}(\bar{K}^{*0}\gamma + K^{*-}\gamma) + \mathcal{N}(K^{*0}\gamma + K^{*+}\gamma)}$$

where \mathcal{N} represents the yield and η is the wrong tag fraction. $|A_{CP}|$ is expected to be less than 1% in the SM. We use only *self-tagging* modes, namely we exclude the $K_S^0\pi^0\gamma$ mode.

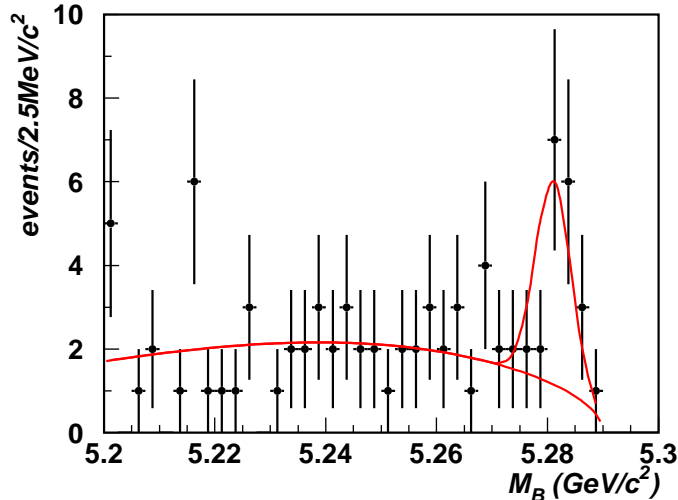


Figure 2: Beam constrained mass spectrum for $B \rightarrow "K_2^*(1430)"\gamma$ candidates.

Thanks to Belle’s good kaon identification devices, the wrong tag fraction η is only 1.2%. We have checked the intrinsic asymmetry in our analysis with an inclusive $K^*(892)$ sample, in which the momentum range of the $K^*(892)$ is adjusted to match our signal. We found that the intrinsic asymmetry is 0.003 ± 0.01 , and is consistent with zero. We extracted the partial yields $\mathcal{N}(\bar{K}^{*0}\gamma + K^{*-}\gamma) = 46.9 \pm 7.3$ and $\mathcal{N}(K^{*0}\gamma + K^{*+}\gamma) = 44.8 \pm 7.1$. We calculated the partial rate asymmetry as

$$A_{CP} = +0.02 \pm 0.11 \pm 0.01$$

and found it is consistent with zero.

2.2 $B \rightarrow K_2^*(1430)\gamma$

We performed a similar analysis with a $K\pi$ invariant mass window of $\pm 100 \text{ MeV}/c^2$ around the nominal $K_2^*(1430)$ mass. We removed the helicity angle from the likelihood ratio in order to check the helicity distribution. This is because there is an overlapping $K^*(1410)$ resonance which has a different spin and thus a different helicity distribution.

We observed $15.6 \pm 4.6_{-0.7}^{+0.6}$ events as shown in Figure 2. In Figure 3, we see a resonance peak in the $K\pi$ invariant mass spectrum. We fitted the helicity distribution with curves for spin-1 and spin-2 hypotheses as shown in Figure 4 and obtained the $K_2^*(1430)\gamma$ fraction to be $(63 \pm 31)\%$ where the error is statistical only. Assuming these are all $K_2^*(1430)\gamma$ events, we quote the branching fraction to be

$$B(B \rightarrow "K_2^*(1430)"\gamma) = (18.9 \pm 5.6 \pm 1.8) \times 10^{-6}.$$

2.3 $B \rightarrow \rho\gamma$

We combined $\pi\pi$ instead of $K\pi$ to search for $B \rightarrow \rho\gamma$. We took a mass window of $\pm 150 \text{ MeV}/c^2$ around the nominal ρ mass. To suppress the $B \rightarrow K^*(892)\gamma$ contribution, we vetoed kaons by a tight kaon-to-pion likelihood ratio cut, and vetoed the $\pi\pi$ combination if its invariant mass

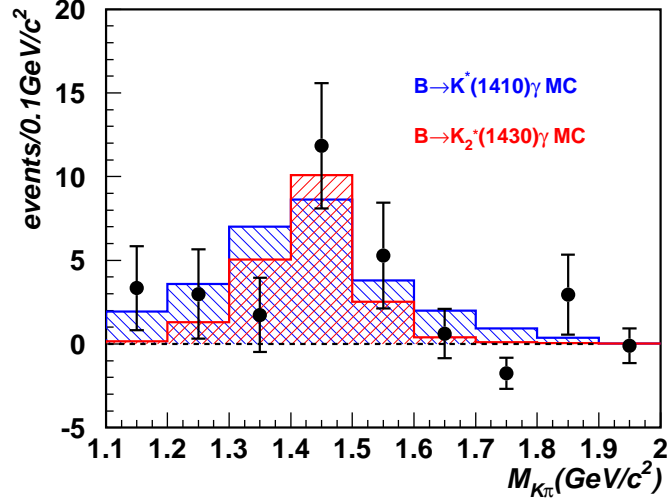


Figure 3: $K\pi$ invariant mass spectrum for $B \rightarrow "K_2^*(1430)"\gamma$ candidates.

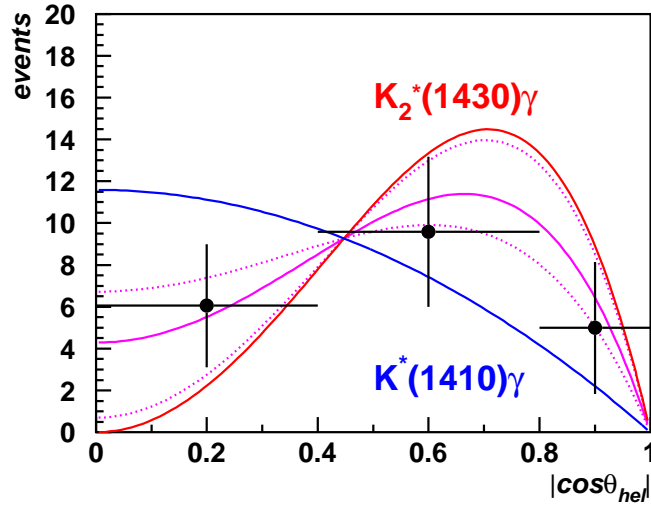


Figure 4: Helicity distribution for $B \rightarrow "K_2^*(1430)"\gamma$ candidates. The result of the fit and the fitting functions $1 - x^2$ and $x^2 - x^4$ are shown as solid lines. Dotted lines are one standard deviation of the fit result.

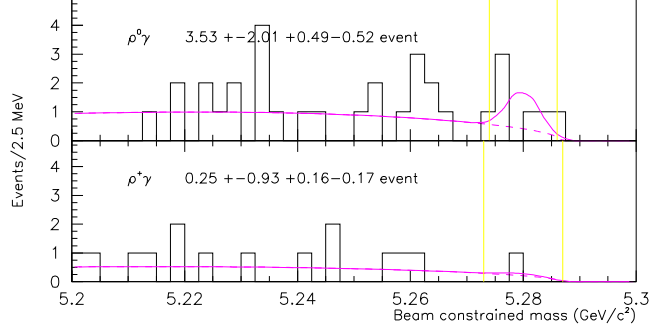


Figure 5: Beam constrained mass spectrum searching for $B \rightarrow \rho^0\gamma$ (top) and $B \rightarrow \rho^+\gamma$ (bottom).

with a $K\pi$ mass hypothesis falls within a window of $50 \text{ MeV}/c^2$ around the nominal $K^*(892)$ mass. The $K^*(892)\gamma$ background contribution is expected to be only 0.4 (0.02) events for $\rho^0\gamma$ ($\rho^+\gamma$).

We observed 6 (1) candidates and a 3.5 ± 2.1 (0.3 ± 0.9) event excess including $K^*(892)\gamma$ background for $B \rightarrow \rho^0\gamma$ ($B \rightarrow \rho^+\gamma$) as shown in Figure 5. Since neither is significant, we set upper limits for the branching fractions $\mathcal{B}(B \rightarrow \rho^0\gamma) < 10.6 \times 10^{-6}$ and $\mathcal{B}(B \rightarrow \rho^+\gamma) < 9.9 \times 10^{-6}$ at 90% confidence level. We also set an upper limit on the $\rho\gamma$ to $K^*(892)\gamma$ fraction, $\frac{\mathcal{B}(B \rightarrow \rho\gamma)}{\mathcal{B}(B \rightarrow K^*(892)\gamma)} < 0.19$ at 90% confidence level.

2.4 $B \rightarrow X_s\gamma$

A semi-inclusive reconstruction is performed by summing up multiple final states. We reconstruct the recoil X_s system from one K^\pm or K_S^0 and one to four pions of which at most one pion can be a π^0 . From X_s and the most energetic photon candidate, we form two independent kinematic variables, M_{bc} and the energy difference ΔE in the $\Upsilon(4S)$ rest frame. We also calculate the angle between the γ and the X_s and require that they are back-to-back in the $\Upsilon(4S)$ rest frame.

We require an X_s candidate to form a vertex with the beam profile constraint except in the case of the $K_S^0\pi^0\gamma$ mode which has no charged track to form a vertex. When there are multiple candidates in an event, we choose the one with the best vertex confidence level. To solve the ambiguities due to neutral particles which do not affect the vertex, we choose the candidate for which the angle between the photon and the X_s is the largest.

For the selected single candidate, we require SFW to be greater than 0.1 to suppress the background from $q\bar{q}$ light quark pair production. We also require the recoil mass to be less than $2.05 \text{ GeV}/c^2$ to suppress the background from other $B\bar{B}$ decays. The SFW distributions for the signal and the $q\bar{q}$ background are shown in Figure 6.

In order to subtract the contribution from $q\bar{q}$ background, which is the main background in this analysis, we use the SFW sideband data (SFW < -1.5) instead of the statistically limited off-resonance data. The SFW variable is tailored not to be correlated with M_{bc} , and hence the M_{bc} distributions in the signal region and in the sideband region are the same.

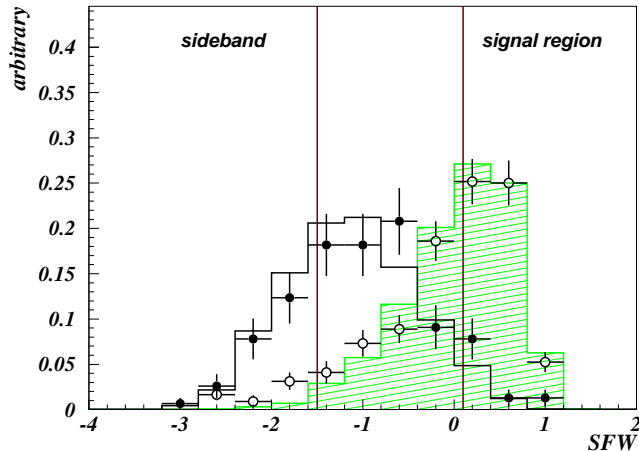


Figure 6: SFW distribution comparison between signal and $q\bar{q}$ background – The signal is concentrated on the higher side while the $q\bar{q}$ background is shifted to the lower side. Histograms are signal MC (hatched) and $q\bar{q}$ MC (open), error bars are $B \rightarrow D\pi$ data (open circles) and off-resonance data (solid circles).

We estimate the $B\bar{B}$ background by using Monte Carlo (MC) and subtract its contribution from the observed data. We then fit the observed M_{bc} spectrum (Figure 7) to be sum of the sideband data and the signal MC floating the normalizations. We find a signal yield of $106.5 \pm 16.8 \pm 5.0$ events, where the first error is statistical and the second is the systematic error in our $q\bar{q}$ background estimation.

In the recoil mass spectrum (Figure 8), we see a clear $K^*(892)$ mass peak and a continuum contribution in the higher resonance region. Therefore, we modeled the recoil mass system as a mixture of $K^*(892)$ and a continuum contribution with the observed ratio of the yields in the $K^*(892)$ region to the continuum region. For the continuum part of the recoil mass spectrum, we adopted a model proposed by Kagan and Neubert [6] with the input b quark mass parameter equal to $4.75 \pm 0.10 \text{ GeV}/c^2$.

We determined the branching fraction

$$\mathcal{B}(B \rightarrow X_s \gamma) = (3.36 \pm 0.53 \pm 0.42_{-0.54}^{+0.50}) \times 10^{-4}$$

where the first error is statistical, the second is systematic and the third is the model error. In Figure 9, we show the measured photon energy spectrum which is corrected for our recoil mass cut. This spectrum can be compared with the model.

3 Summary

The measured branching fractions for $B \rightarrow K^*(892)\gamma$ and $B \rightarrow X_s\gamma$ are consistent with the other experimental results [7] and/or the SM prediction [3]. We do not see a deviation from the SM prediction in the partial rate asymmetry in $B \rightarrow K^*(892)\gamma$, either.

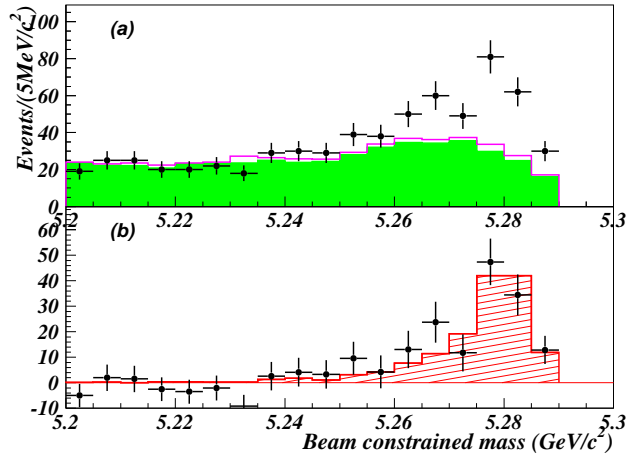


Figure 7: Beam constrained mass spectrum for $B \rightarrow X_s \gamma$: (a) observed spectrum (points with error bars) and background contributions; the total background is the open histogram and the $q\bar{q}$ contribution is the solid part. (b) background subtracted data (points with error bars) and signal MC prediction (hatched histogram).

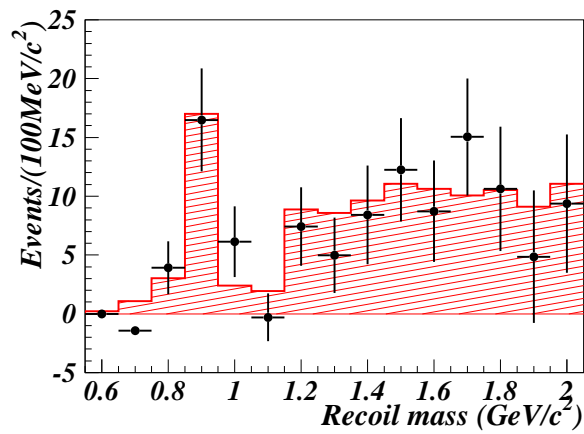


Figure 8: Recoil mass spectrum for $B \rightarrow X_s \gamma$. Data points (points with error bars) are compared with signal MC (hatched histogram).

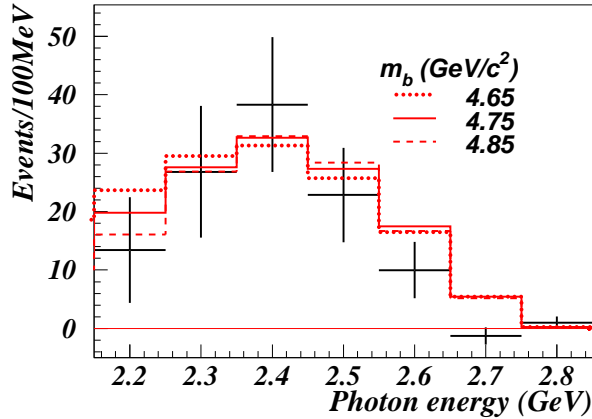


Figure 9: Photon energy spectrum for $B \rightarrow X_s \gamma$. Data points (points with error bars) are compared to signal MC (histograms) with three different b quark mass parameter values.

We observed a significant excess of $B \rightarrow (K\pi)\gamma$ in the $K_2^*(1430)$ resonance region. The contributions from $K_2^*(1430)$ and $K^*(1410)$ are not disentangled yet.

We have not observed $B \rightarrow \rho\gamma$ decays. The upper limit for its branching fraction has been updated from what we reported previously [8].

References

- [1] The Belle Collaboration, K. Abe et al., “The Belle Detector”, KEK Progress Report 2000-4 (2000), to be published in Nucl. Instr. Meth. A.
- [2] KEK accelerator group, “KEKB B-Factory Design Report”, KEK Report 95-7 (1995), unpublished.
- [3] K. Chetyrkin, M. Misiak, M. Münz, Phys. Lett. **B400**, 206, (1997); Erratum ibid. **B425**, 414, (1998)
- [4] For example, F. Borzumati, C. Greub, Phys. Rev. **D58**, 074004, (1998); M. Ciuchini, G. Degrassi, P. Gambino, G. F. Giudice, Nucl. Phys **B534**, 3, (1998); C. Bobeth, M. Misiak, J. Urban, Nucl. Phys. **B567**, 153, (2000)
- [5] The Belle Collaboration, K. Abe et al., “A Measurement of the Branching Fraction for the Inclusive $B \rightarrow X_s \gamma$ Decays with Belle”, hep-ex/0103042 (2001), submitted to Phys. Lett. B.
- [6] A. L. Kagan, M. Neubert, Eur. Phys. J. **C7**, 5 (1999).
- [7] For the $B \rightarrow X_s \gamma$ branching fraction, The CLEO collaboration, Phys. Rev. Lett. **74**, (1995); The ALEPH collaboration, Phys. Lett. **B429**, (1998);

For the $B \rightarrow K^*(892)\gamma$ branching fraction, The CLEO collaboration, Phys. Rev. Lett. **84**, 5283 (2000).

- [8] M. Nakao (the Belle collaboration), “Studies of Radiative B Meson Decays with Belle”, Proceedings of the 30th International Conference on High Energy Physics, July 2000, Osaka.